

ViewFormer: View Set Attention for Multi-view 3D Shape Understanding

Hongyu Sun Yongcai Wang Peng Wang Xudong Cai Deying Li
 Renmin University of China
 No. 59, Zhongguancun Street, Haidian District, Beijing 100872, China
 {sunhongyu, ycw, peng.wang, xudongcai, deyingli}@ruc.edu.cn

Abstract

This paper presents ViewFormer, a simple yet effective model for multi-view 3d shape recognition and retrieval. We systematically investigate the existing methods for aggregating multi-view information and propose a novel “view set” perspective, which minimizes the relation assumption about the views and releases the representation flexibility. We devise an adaptive attention model to capture pairwise and higher-order correlations of the elements in the view set. The learned multi-view correlations are aggregated into an expressive view set descriptor for recognition and retrieval. Experiments show the proposed method unleashes surprising capabilities across different tasks and datasets. For instance, with only 2 attention blocks and 4.8M learnable parameters, ViewFormer reaches 98.8% recognition accuracy on ModelNet40 for the first time, exceeding previous best method by 1.1%. On the challenging RGBD dataset, our method achieves 98.4% recognition accuracy, which is a 4.1% absolute improvement over the strongest baseline. ViewFormer also sets new records in several evaluation dimensions of 3D shape retrieval defined on the SHREC’17 benchmark.

1. Introduction

With the advancement of 3D perception devices and methods, 3D assets (point clouds, meshes, RGBD images, CAD models, etc.) become more and more common in daily life and industrial production. 3D object recognition and retrieval are basic requirements for understanding the 3D contents and the development of these technologies will benefit downstream applications like VR/AR/MR, 3D printing, and autopilot. Existing methods for 3D shape analysis can be roughly divided into three categories according to the input representation: point-based [32, 34, 45, 41, 48, 57, 26, 52, 50, 58, 30], voxel-based [49, 31, 33, 59], and view-based methods [39, 40, 13, 44, 11, 17, 16, 7, 28, 46, 47, 56, 12, 14]. Among them, view-based methods recognize a 3D object based on its rendered or projected im-

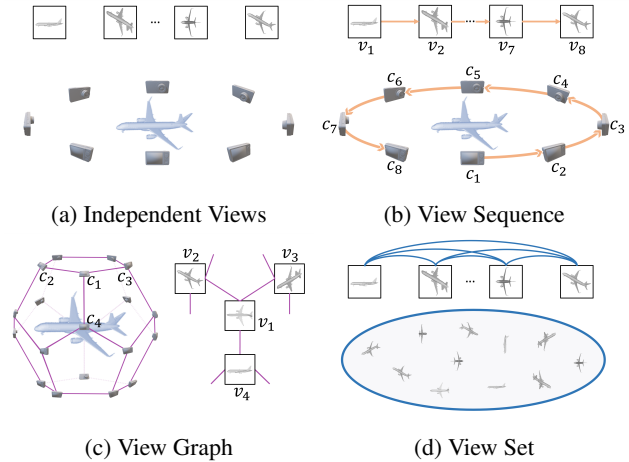


Figure 1: A division for multi-view 3D shape analysis methods based on how they organize views and aggregate multi-view information. View Set is the proposed perspective that the views of a 3D shape are organized in a set.

ages, termed *multiple views*. Generally, methods in this line [40, 46, 6, 51] outperform the point- and voxel-based counterparts [33, 52, 50, 58, 30]. On one hand, view-based methods benefit from massive image datasets and the advances in image recognition over the past decade. On the other hand, the multiple views of a 3D shape contain richer visual and semantic signals than the point or voxel form. For example, one may not be able to decide whether two 3D shapes belong to the same category by observing them from one view, but the answer becomes clear after watching other views of these shapes. The example inspires a central problem, e.g., how to exploit multi-view information effectively for a better understanding of 3D shape.

This paper systematically investigates existing methods on how they aggregate the multi-view information and the findings are summarized in Figure 1. In the early stage, MVCNN [39] and its follow-up work [40, 13, 55, 44, 54] independently process multiple views of a 3D shape by a shared CNN. The extracted features are fused with pooling operation or some variants to form a compact 3D shape descriptor. We group these methods into *Independent Views*

in Figure 1a. Although the simple design made them stand out at the time, they did not take a holistic perspective to the multiple views of a 3D shape and the information flow among views was insufficient. In the second category, a growing number of methods model multiple views as a sequence [17, 16, 7, 28, 53], which are grouped into *View Sequence* in Figure 1b. They deploy RNNs, like GRU [9] and LSTM [19], to learn the view relations. However, a strong assumption behind *View Sequence* is that the views are collected from a circle around the 3D shape. In many cases, the assumption may be invalid since the views can be rendered from random viewpoints, so they are unordered. To alleviate this limitation, later methods describe views with a more general structure, e.g., graph [46, 47] or hyper-graph [56, 12, 14], and develop graph convolution networks (GCNs) to propagate and integrate view features, called *View Graph* in Figure 1c. Methods in this category show both flexibility and promising performance gains, whereas they require constructing a view graph according to the positions of camera viewpoints. But sometimes the viewpoints may be unknown and graph construction introduces additional computation overheads. In addition, message propagation between remote nodes on the view graphs may not be straightforward. Some other methods explore rotations [22, 11], multi-layered height-maps representations [37], view correspondences [51], viewpoints selection [15] when analyzing 3D shapes. They can hardly be divided into the above categories, but multi-view correlations in their pipelines still need to be enhanced.

By revisiting existing works, two ingredients are found critical for improving multi-view 3D shape analysis. The first is how to organize the views so that they can communicate with each other flexibly and freely. The second is how to integrate multi-view information effectively. It is worth noting that the second ingredient is usually coupled with the first, just like GCNs defined on the view graphs, and RNNs defined on the view sequences. In this paper, we present a novel perspective that multiple views of a 3D shape are organized into a *View Set* in Figure 1d, where elements are permutation invariant, which is consistent with the fact that 3D shape understanding is actually not dependent on the order of input views. For example, in Figure 1b, whether the side view is placed first, middle or last in the inputs, the recognition result should always be `airplane`. Unlike existing methods analyzed above, this perspective also makes no assumptions about the correlations of views, which is more flexible and practical in real-world applications. Instead, to aggregate multi-view information, a view set attention model, ViewFormer, is devised to learn the pairwise and higher-order relations among the views adaptively. The attention architecture is a natural choice because it aligns with the view set characteristics. First, the attention mechanism is essentially a set operator and inherently good at cap-

turing correlations between the elements in a set. Second, this mechanism is flexible enough that it makes minimal assumptions about the inputs, which matches our expectation that there are no predefined relations or additional requirements for views.

The proposed model has four components: *Initializer*, *Encoder*, *Transition*, and *Decoder*. *Initializer* initializes the representations of views. *Encoder* is adapted from standard Transformer encoder [43] with specific modifications. i) The position encodings of input views are removed since views are permutation invariant. ii) The class token is removed because it is irrelevant to capturing the correlations of views in the set. iii) The number of attention blocks is greatly reduced as the size of a view set is relatively small (≤ 20 in most cases) so it is unnecessary to employ deeper blocks. *Transition* summarizes the learned correlations into a compact *View Set Descriptor (VSD)* to express the ViewFormer’s understanding of the 3D shape. *Decoder* is designed towards downstream tasks, such as recognition and retrieval. The simple designs around the view set show not only great flexibility but also powerful capability for 3D shape understanding. New records are obtained by ViewFormer in downstream tasks of 3D shape recognition and retrieval. In summary, the contributions of this paper include:

- A systematical investigation of existing methods in aggregating multi-views for 3D shape understanding. A novel perspective is proposed that multiple views are incorporated in a *View Set*. And a simple yet effective view set attention model, ViewFormer, is designed to adaptively capture pairwise and higher-order correlations among the views for better understanding.
- Extensive evaluations demonstrate the superb performances of the proposed approach. The recognition accuracy on ModelNet40 can reach as high as 98.8%, surpassing all existing methods. On the challenging RGBD dataset, ViewFormer achieves 98.4% classification accuracy, which is a 4.1% absolute improvement over previous state-of-the-art. ViewFormer-based 3D shape retrieval sets new records in several evaluation dimensions on SHREC’17 benchmark.
- Ablation studies shed light on the various sources of performance gains for 3D shape understanding and the visualizations provide some insightful conclusions.

2. Related Work

In this section, we review the multi-view 3D shape analysis methods and explore the deployment of set and attention in these methods.

Multi-view 3D Shape Analysis. Existing methods aggregate multi-view information for 3D shape understanding in

different ways. (1) *Independent Views*. Early work like MVCNN series [39] and its follow-up [40, 13, 55, 44, 54] extract view features independently using a shared CNN, then fuse the extracted features using the pooling operation or some variants. The simple strategy may discard a lot of useful information and the views are not well treated as a whole thus information flow among views needs to be increased. (2) *View Sequence*. Researchers perceive the problems and propose various descriptions to incorporate multiple views of a 3D shape into a specific data structure. For example, RNN-based methods [17, 16, 7, 53, 28, 6] are proposed to operate on the view sequence. (3) *View Graphs*. The graph-based models [12, 56, 46, 47, 14] assume the relations among views as graphs and develop GCNs to capture multi-view interaction. However, message propagation on view graphs may not be straightforward and graph construction leads to additional overheads. (4) This paper presents a flexible and practical perspective, *View Set*, which neither makes assumptions about views nor introduces additional overheads. Based on that, a view set attention model is devised to adaptively integrate the correlations for all view pairs. Some other methods also explore rotations [22, 11], multi-layered height-maps representations [37], view correspondences [51], viewpoints selection [15] when analyzing 3D shapes. Their multi-view interaction still needs to be strengthened.

Set in Multi-view 3D Shape Analysis. Previous works also mention “set” in multi-view 3D shape analysis. But they basically refer to different concepts from the proposed one. For instance, RCPCNN [44] introduces a dominant set clustering and pooling module to improve MVCNN [39]. Johns *et al.* decompose a sequence of views into a set of view pairs. They classify each pair independently and weigh the contribution of each pair [21]. MHBN [55] considers patches-to-patches (set-to-set) similarity of different views and aggregates local features using bilinear pooling. Yu *et al.* extend MHBN by introducing VLAD layer [54]. The basic idea is to calculate the similarity between two sets of local patches, while our view set idea provides a foundation for adaptively learning inter-view attentions.

Attention in Multi-view 3D Shape Analysis. The attention mechanisms have been embedded in existing multi-view 3D shape recognition methods, but they vary in motivation, practice and effectiveness. VERAM [7] uses a recurrent attention model to select a sequence of views to classify 3D shapes adaptively. SeqViews2SeqLabels [17] introduces the attention mechanism to increase the discriminative ability for the RNN-based model and reduces the effect of selecting the first view position. 3D2SeqViews [16] proposes hierarchical attention to incorporate view-level and class-level importance for 3D shape analysis. Nevertheless, there are two points worth noting for the attention of the above methods. First, the attention operation in these

methods differs from multi-head self-attention in standard Transformer [43]. Second, the dedicated designed attention does not seem to produce satisfactory results since the highest recognition accuracy they achieve on ModelNet40 is 93.7%, whereas our solution reaches 99.0% on the same dataset. Recent work MVT [6] also explores the attention architecture for view-based 3D recognition. It is inspired by the success of ViT [10] in image recognition and wants to strengthen view-level communications with patch-level correlations. MVT deploys a ViT to extract patch-level features for all images and adopts another ViT to learn the correlations for all views. However, ViewFormer shows it is unnecessary to take the patch-level interactions into account to achieve the best results, thus the computation budgets are considerably reduced compared to MVT.

3. ViewFormer

In this section, we firstly formulate the problem of multi-view 3D shape recognition and retrieval based on the view set, then elaborate on the devised model and how it handles a set of views.

3.1. Problem Formulation

View Set. The views of a 3D shape refer to the rendered or projected RGB images from it. For example, a 3D shape \mathcal{S} corresponds to views $v_1, v_2, \dots, v_M \in \mathbb{R}^{H \times W \times C}$, where M is the number of views and $H \times W \times C$ indicates the image size. In our perspective, the views of \mathcal{S} simply form a set $\mathcal{V} = \{v_1, v_2, \dots, v_M\}$, where elements are permutation invariant. Thus \mathcal{V} can be instantiated as a random permutation of the views. This perspective matches the basic fact that views can be generated from random viewpoints in the real world. It neither assumes relations for views nor introduces additional overheads, distinguished from previous methods analyzed above.

3D Shape Recognition & Retrieval. In many cases [38], 3D shape retrieval can be regarded as a classification problem. It aims to find the most relevant shapes to the query. Meanwhile, the relevance is defined according to the ground truth class and subclass of the query, which means if a retrieved shape has the same class and subclass as the query, they match perfectly. Therefore, the tasks of 3D shape recognition and retrieval can be unified by predicting a category distribution $\hat{\mathbf{y}} \in \mathbb{R}^K$ of the target shape \mathcal{S} , where K is the number of 3D shape categories. In this paper, we design a simple yet effective view set attention model \mathcal{F} to predict the distribution. The input of \mathcal{F} is a view set $\mathcal{V} \in \mathbb{R}^{M \times H \times W \times C}$, corresponding to the shape \mathcal{S} . The procedure is formulated by Eq. 1 and the details are dissected in the next section.

$$\hat{\mathbf{y}} = \mathcal{F}(\mathcal{V}) \quad (1)$$

3.2. View Set Attention Model

The proposed view set attention model, ViewFormer, is to adaptively grasp pairwise and higher-order correlations among views in the set. And it summarizes the learned correlations into an expressive descriptor for 3D shape analysis. ViewFormer is more straightforward in modeling the correlations of views than graph-based methods because it explicitly computes the attention scores for all view pairs. The overall architecture of ViewFormer includes four modules: Initializer, Encoder, Transition, and Decoder.

Initializer. This module initializes the feature representations of views in \mathcal{V} to feed Encoder. We denote the module as Init and it converts $v_i \in \mathbb{R}^{H \times W \times C}$ to the feature representation $z_i \in \mathbb{R}^D$, where D is the feature dimension. After this module, the view set $\mathcal{V} = \{v_1, \dots, v_i, \dots, v_M\}$ is transformed to the initialized feature set $\mathbf{z}^0 = \{z_1, \dots, z_i, \dots, z_M\}$, shown in Eq. 2.

$$\mathbf{z}^0 = \text{Init}(\mathcal{V}) \quad (2)$$

Init has various choices, such as linear projection, MLP, CNN or ViT. The complexity and efficiency are tradeoffs. A simple linear projection from a $224 \times 224 \times 3$ view to a 512-dimensional vector will result in $\sim 77\text{M}$ parameters in Init, and the MLP will produce more. Some work [55, 54, 6] also consider fine-grained patch-level features within each view and then combine them with the view-level ones. But this mean is computation expensive. In ViewFormer, we adopt lightweight CNNs (e.g., AlexNet [24], ResNet18 [18]) as Init because they are efficient and good at image feature extraction.

Encoder. This module that consists of consecutive attention blocks is adapted from standard Transformer [43] encoder with the following modifications. First, the position encodings are removed since the views should be unaware of their order in the view set. Second, the class token is removed because it is irrelevant to the target of modeling the correlations of views in the set. Third, the number of attention blocks is greatly reduced as the size of a view set is relatively small (≤ 20 in most cases), so employing very complex encoder is inappropriate.

Encoder receives the initialized view feature set $\mathbf{z}^0 \in \mathbb{R}^{M \times D}$ and processes them with L attention blocks. Each attention block stacks the multi-head self-attention[43] (MSA) and MLP layers with residual connections. LayerNorm (LN) is deployed before MSA and MLP, whereas Dropout is applied after them. The feature interaction is explicitly calculated for all view pairs in each attention block and by going deeper, the higher-order correlations are learned. The procedure in the ℓ th block is summarized by Eq. 3 and 4.

$$\hat{\mathbf{z}}^\ell = \text{Dropout}(\text{MSA}(\text{LN}(\mathbf{z}^{\ell-1}))) + \mathbf{z}^{\ell-1} \quad \ell = 1 \dots L \quad (3)$$

$$\mathbf{z}^\ell = \text{Dropout}(\text{MLP}(\text{LN}(\hat{\mathbf{z}}^\ell))) + \hat{\mathbf{z}}^\ell \quad \ell = 1 \dots L \quad (4)$$

Transition. The last attention block of Encoder outputs the collective correlations of multiple views $\mathbf{z}^L \in \mathbb{R}^{M \times D}$ and we convert the learned correlations into a view set descriptor by the Transition module (Transit). The pooling operations are typical options in existing methods [39, 44, 13, 55, 54]. In this paper, we concatenate (Concat) the results of max and mean pooling along the first dimension of \mathbf{z}^L to stabilize the optimization and the operation does not introduce learnable parameters. The output is denoted as $\mathbf{t}^L \in \mathbb{R}^{2D}$ in Eq. 5.

$$\mathbf{t}^L = \text{Transit}(\mathbf{z}^L) = \text{Concat}(\text{Max}(\mathbf{z}^L), \text{Mean}(\mathbf{z}^L)) \quad (5)$$

Decoder. This module decodes the view set descriptor \mathbf{t}^L to a 3D shape category distribution $\hat{\mathbf{y}} \in \mathbb{R}^K$. In ViewFormer, we show the decoder can be designed extremely lightweight, as light as a single Linear. We also make a look into the performance of heavier heads, such as 2- or 3-layer MLP preceded by BatchNorm (BN) and ReLU in each layer. We find both of them work well, reflecting the summarized view set descriptor \mathbf{t}^L is highly expressive.

$$\hat{\mathbf{y}} = \text{Decoder}(\mathbf{t}^L) \quad (6)$$

By combining the simple design of each component, the proposed method exhibits powerful capabilities across different datasets and tasks, supported by systematic experiments and extensive ablation studies in the next section.

4. Experiments

In this section, firstly, we explain the experimental settings of ViewFormer. Then the proposed method is evaluated on 3D shape recognition and retrieval tasks. Thirdly, we conduct controlled experiments to justify the design choices of ViewFormer. Finally, visualizations are presented for a better understanding of the method.

4.1. Basic Configurations

Architecture. For Initializer, we adopt lightweight CNNs. There are several candidates (AlexNet, ResNet18, etc.) and we will compare them later. The view $z_i \in \mathcal{V}$ is mapped to a 512-dimensional vector through Initializer. For Encoder, there are $L=4$ attention blocks and within each block, the MSA layer has 8 attention heads and the widening factor of the MLP hidden layer is 2. The Transition module converts the collective correlations in \mathbf{z}^L into a 1024-dimensional descriptor. Finally, the descriptor is projected to a category distribution by Decoder, which is a 2-layer MLP of shape $\{1024, 512, K\}$. The design choices are verified by ablated studies in Section 4.4.

Optimization. The loss function is defined as CrossEntropyLoss for 3D shape recognition. Following previous

Method	Input	Class Acc. (%)	Inst. Acc. (%)
3DShapeNets [49]		77.3	–
VoxNet [31]	Voxels	83.0	–
VRN Ensemble [4]		–	95.5
MVCNN-MR [33]		91.4	93.8
PointNet++ [34]		–	91.9
DGCNN [45]		90.2	92.9
RSCNN [26]	Points	–	93.6
KPConv [41]		–	92.9
CurveNet [50]		–	93.8
PointMLP [30]		91.3	94.1
MVCNN [39]		90.1	90.1
MVCNN-new [40]		92.4	95.0
MHBN [55]		93.1	94.7
GVCNN [13]		90.7	93.1
RPCNN [44]		–	93.8
RN [53]		92.3	94.3
3D2SeqViews [16]		91.5	93.4
SV2SL [17]		91.1	93.3
VERAM [7]		92.1	93.7
Ma <i>et al.</i> [29]		–	91.5
iMHL [56]	Views	–	97.2
HGNN [12]		–	96.7
HGNN+ [14]		–	96.9
View-GCN [46]		96.5	97.6
View-GCN++ [47]		96.5	97.6
DeepCCFV [20]		–	92.5
EMV [11]		92.6	94.7
RotationNet [22]		–	97.4
MVT [6]		–	97.5
CARNet [51]		–	97.7
MVTN [15]		92.2	93.5
ViewFormer	Views	98.9	98.8

Table 1: Comparison of 3D shape recognition on ModelNet40. The best score is in bold black and the second best is in blue. The convention is kept in the following tables.

methods [40, 46], the learning is divided into two stages. In the first stage, the Initializer is individually trained on the target dataset for 3D shape recognition. The purpose is to provide good initializations for views. In the second stage, the pre-trained Initializer is loaded and jointly optimized with other modules on the same dataset. Experiments show this strategy will significantly improve performance in a shorter period. More explanations about network optimization and evaluations of learning efficiency are provided in the supplementary material.

Method	Input	Class Acc. (%)	Inst. Acc. (%)
3D2SeqViews [16]		94.7	94.7
SV2SL [17]		94.6	94.7
VERAM [7]	Views	96.1	96.3
RotationNet [22]		–	98.5
CARNet [51]		–	99.0
MVT [6]		–	99.3
ViewFormer	Views	100.0	100.0

Table 2: Comparison of 3D shape recognition on ModelNet10.

Method	#Views	Inst. Acc. (%)
CFK [8]	≥ 120	86.8
MMDCNN [35]	≥ 120	89.5
MDSICNN [1]	≥ 120	89.6
MVCNN [39]	12	86.1
RotationNet [22]	12	89.3
View-GCN(ResNet18) [46]	12	94.3
View-GCN(ResNet50) [46]	12	93.9
ViewFormer(ResNet18)	12	98.4
ViewFormer(ResNet50)	12	95.6

Table 3: Comparison of 3D shape recognition on RGBD.

4.2. 3D Shape Recognition

Datasets & Metrics. We conduct 3D shape recognition on three datasets, ModelNet10 [49], ModelNet40 [49] and RGBD [25]. ModelNet10 has 4,899 CAD models in 10 categories and ModelNet40 includes 12,311 objects across 40 categories. For ModelNet10/40, we use their rendered versions as in previous work [40, 46], where each object corresponds to 20 views. RGBD is a large-scale, hierarchical multi-view object dataset [25], containing 300 objects organized into 51 classes. In RGBD, we use 12 views for each 3D object as in [22, 46]. Two evaluation metrics are computed for 3D shape recognition: mean class accuracy (Class Acc.) and instance accuracy (Inst. Acc.). We record the best results of these metrics during optimization.

Results. Table 1 compares representative methods on ModelNet40 and these methods have different input formats: voxels, points and views. ViewFormer achieves 98.9% mean class accuracy and 98.8% overall accuracy, surpassing the voxel- and point-based counterparts. Also, it sets new records in view-based methods. For example, compared to early works [39, 40, 55, 13, 44] that aggregate multi-view information independently by pooling or some variants, ViewFormer exceeds their instance accuracies by 3.8% at least. ViewFormer also significantly improves the

Method	micro					macro				
	P@N	R@N	F1@N	mAP	NDCG	P@N	R@N	F1@N	mAP	NDCG
ZFDR	53.5	25.6	28.2	19.9	33.0	21.9	40.9	19.7	25.5	37.7
DeepVoxNet	79.3	21.1	25.3	19.2	27.7	59.8	28.3	25.8	23.2	33.7
DLAN	81.8	68.9	71.2	66.3	76.2	61.8	53.3	50.5	47.7	56.3
GIFT [2]	70.6	69.5	68.9	64.0	76.5	44.4	53.1	45.4	44.7	54.8
Improved GIFT [3]	78.6	77.3	76.7	72.2	82.7	59.2	65.4	58.1	57.5	65.7
ReVGG	76.5	80.3	77.2	74.9	82.8	51.8	60.1	51.9	49.6	55.9
MVFusionNet	74.3	67.7	69.2	62.2	73.2	52.3	49.4	48.4	41.8	50.2
CM-VGG5-6DB	41.8	71.7	47.9	54.0	65.4	12.2	66.7	16.6	33.9	40.4
MVCNN [39]	77.0	77.0	76.4	73.5	81.5	57.1	62.5	57.5	56.6	64.0
RotationNet [22]	81.0	80.1	79.8	77.2	86.5	60.2	63.9	59.0	58.3	65.6
View-GCN [46]	81.8	80.9	80.6	78.4	85.2	62.9	65.2	61.1	60.2	66.5
View-GCN++ [47]	81.2	79.9	80.0	77.5	83.9	61.2	65.8	61.1	59.0	63.8
ViewFormer	81.6	82.0	81.3	78.4	81.7	64.5	65.4	62.9	60.6	67.5

Table 4: Comparison of 3D shape retrieval on ShapeNet Core55.

results of methods built on view sequence, such as RelationNet [53], 3D2SeqViews [16], SeqViews2SeqLabels [17], VERAM [7]. Methods defined on view graph and hypergraph achieve decent performances [56, 12, 14, 46, 47] because of enhanced information flow among views. ViewFormer still outreaches the strongest baseline of this category, increasing 2.4% Class Acc. and 1.2% Inst Acc. over View-GCN [46].

Table 2 presents the recognition results on ModelNet10. Although the dataset is relatively easy and previous methods can work very well (as high as 99.3% Inst. Acc.), it is a bit surprising that ViewFormer successfully recognizes all shapes in the test set and obtains 100% accuracy. Previous best method MVT [6] combines patch- and view-level feature communications by applying ViT [10] twice. ViewFormer achieves better results without taking patch-level interaction into account.

Table 3 records the comparison with related work on the challenging RGBD [25] dataset. The dataset designs 10-fold cross-validation for multi-view 3D object recognition. We follow this setting and report the average instance accuracy of 10 folds. ViewFormer shows consistent improvements over View-GCN under the same Initializer. Especially, it gets 98.4% accuracy that is a 4.1% absolute improvement over the runner-up, suggesting ViewFormer can produce more expressive shape descriptors when dealing with challenging cases.

4.3. 3D Shape Retrieval

Datasets & Metrics. 3D shape retrieval aims to find a rank list of shapes most relevant to the query shape in a given dataset. We conduct this task on ShapeNet Core55 [5, 38].

The dataset is split into train/val/test set and there are 35764, 5133 and 10265 meshes, respectively. 20 views are rendered for each mesh as in [22, 46]. According to the SHREC’17 benchmark [38], the rank list is evaluated based on the ground truth category and subcategory. If a retrieved shape in a rank list has the same category as the query, it is positive. Otherwise, it is negative. The evaluation metrics include micro and macro version of P@N, R@N, F1@N, mAP and NDCG. Here N is the length of returned rank list and its maximum value is 1,000 according to the requirement. Please refer to [38] for more details about the metrics.

Retrieval. We generate the rank list for each query shape in two steps. First, ViewFormer is trained to recognize the shape categories in ShapeNet Core55 [5]. We retrieve shapes that have the same predicted class as the query Q and rank the retrieved shapes according to class probabilities in descending order, resulting in L_1 . Second, we train another ViewFormer to recognize the shape subcategories of ShapeNet Core55 [5], then re-rank L_1 to ensure shapes that have same predicted subcategory as the query Q rank before shapes that are not in same subcategory with Q and keep the remaining unchanged, resulting in L_2 , which is regarded as the final rank list for the query Q .

Results. ViewFormer is compared with the methods that report results on SHREC’17 benchmark [38], shown in Table 4. The methods in the first three rows use voxel representations of 3D shapes as inputs, while the remaining methods exploit multiple views. The overall performances of view-based methods are better than voxel-based ones. Previously, View-GCN achieved state-of-the-art results by enhancing view interaction and aggregating multi-view in-

formation on on view-graphs. But experiments show ViewFormer goes beyond View-GCN in terms of micro-version R@N, F1@N and mAP as well as macro-version P@N, F1@N, mAP and NDCG. For example, we achieve at least 1.0% absolute improvements for both micro-version R@N and macro-version NDCG over View-GCN.

4.4. Ablation Studies

We conduct a series of controlled experiments to verify the choices in ViewFormer design. The used dataset is ModelNet40.

Initializer. We explore different means to initialize view representations, including shallow convolution operations and lightweight CNNs. The idea of shallow convolution operation is inspired by the image patch projection (1x1 Conv) in ViT [10] and the specific configurations are explained in the supplementary material. Table 5 compares their recognition accuracies. We observe that initializations by 1- and 2-layer convolution operations do not yield satisfactory results. Instead, lightweight CNNs work well, especially when receiving the initialized features by AlexNet and jointly optimizing with other modules, ViewFormer reaches 98.9% class accuracy and 98.8% overall accuracy, both are new records on ModelNet40. By default, AlexNet serves as the Initializer module.

Initializer	#Params (M)	Class Acc. (%)	Inst. Acc. (%)
1-layer Conv	102.8	90.1	92.5
2-layer Conv	12.9	88.9	93.7
alexnet	42.3	98.9	98.8
resnet18	11.2	96.7	97.6
resnet34	21.3	96.9	97.1

Table 5: Ablation study: choices for Initializer.

Position Encoding. According to the view set perspective, ViewFormer should be unaware of the order of elements in the view set so we remove the position encoding from the devised encoder. We examine this design in Table 6. The results show if learnable position embeddings are forcibly injected into the initialized view features to make the model position-aware, the performance will be hindered, dropping by 0.5% for class accuracy and 0.3% for overall accuracy.

Class Token. Unlike standard Transformer [43], the proposed method does not insert the class token into the inputs since it is irrelevant to the target of capturing the correlations among views in the set. This claim is supported by the results in Table 6, which shows that inserting the class token results in decreasing recognition accuracies.

Number of Attention Blocks. In ViewFormer, the number of attention blocks in Encoder is considerably compressed

Variants	Class Acc. (%)	Inst. Acc. (%)
w/ pos. enc.	98.4	98.5
w/o pos. enc.	98.9	98.8
w/ cls. token	98.8	98.5
w/o cls. token	98.9	98.8

Table 6: Ablation study: position encoding and class token.

Module	#Params (M)	Inst. Acc. (%)
AlexNet	42.3	85.1
+ 2 Attn. Blocks	4.8	98.8
+ 4 Attn. Blocks	9.0	98.8
+ 6 Attn. Blocks	13.2	98.3

Table 7: Ablation study: number of attention blocks.

because the size of a view set is relatively small and it is unnecessary to deploy a deeper encoder to model the interactions between the views in the set. The results in Table 7 demonstrate the encoder can be highly lightweight, as light as two attention blocks, but with outstanding performance compared to existing methods. The results also indicate increasing the attention blocks does not receive gains but additional parameters and overheads.

Transition. We investigate three kinds of operations for the Transition module. The results are reported in Table 8. We find the simple pooling operations (Max and Mean) can work well (98.0+% Acc.) and both outreach the performances of previous state of the art. By concatenating the outputs of max and mean pooling, the optimization is more stable and the overall accuracy is lifted to 98.8%. It is worth noting that the same pooling operations are adopted by MVCNN [39] and its variants [40, 13, 55, 44, 54], but their accuracies are up to 95.0%, implying that the view set descriptors learned by our encoder are more informative.

Transition	Class Acc. (%)	Inst. Acc. (%)
Max pooling	99.1	98.5
Mean pooling	98.5	98.5
Concat(Max&Mean)	98.9	98.8

Table 8: Ablation study: choices for Transition.

Decoder. The decoder projects the view set descriptor to a shape category distribution. The choices for the decoder are compared in Table 9. ViewFormer with a decoder of a single Linear can recognize 3D shapes at 98.1% instance accuracy, which outperforms all existing methods and again, reflects the summarized view set descriptor is highly discriminative. The advantage is enlarged when the decoder is

Decoder	Class Acc. (%)	Inst. Acc. (%)
1-layer	97.9	98.1
2-layer	98.9	98.8
3-layer	98.5	98.5

Table 9: Ablation study: choices for Decoder.

deepened to a 2-layer MLP. However, further tests show it is unnecessary to exploit deeper transformations.

We conduct additional analysis of the proposed model, including the training strategy, running efficiency, the number of views, the structure of the view set encoder and the effect of patch-level correlations, please refer to the supplementary material for more insights.

4.5. Visualization

Multi-view Attention Map. For better understanding, we visualize the attention map of eight views of a 3D airplane in Figure 2. The attention scores are taken from the outputs of the last attention block of our model. The map indicates the 6th view is representative since it receives more attentions from other views. On the other hand, we can manually infer the 6th view is representative based on the visual appearances of these views. The results reflect that ViewFormer can adaptively capture the multi-view correlations and assign more weights to the representative views for recognition.

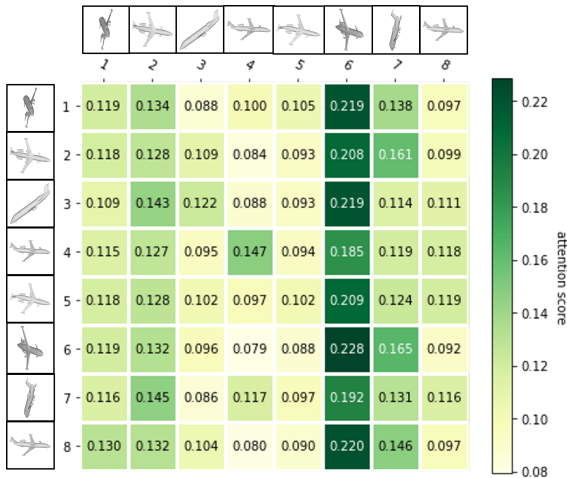


Figure 2: Visualization of the attention scores for 8 views of a 3D airplane.

3D Shape Recognition. We visualize the feature distribution for different shape categories on ModelNet10, ModelNet40 and RGBD using t-SNE [42], shown in Figure 3. It shows different shape categories of different datasets are successfully distinguished by the proposed method, demon-

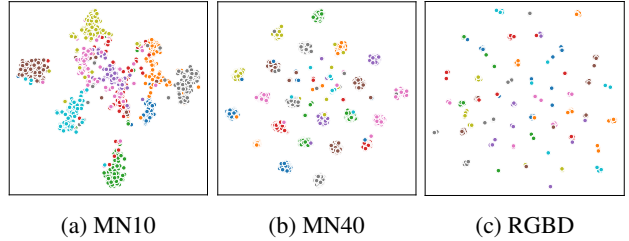


Figure 3: Visualization of 3D shape feature distribution on ModelNet10 (MN10), ModelNet40 (MN40) and RGBD.

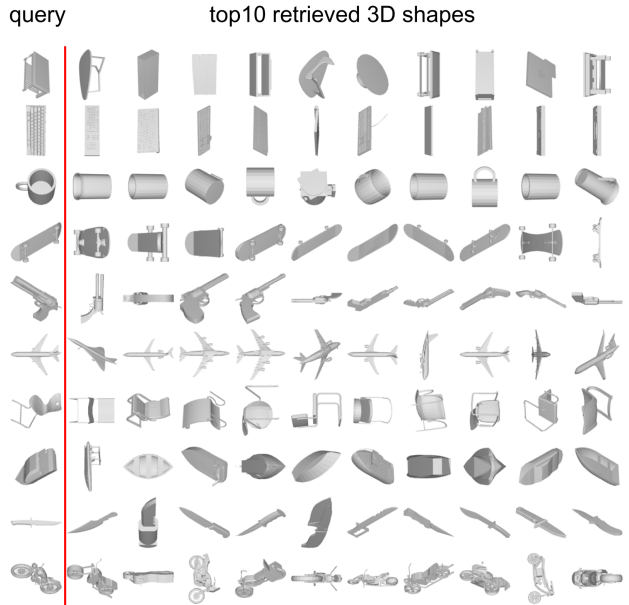


Figure 4: Visualization of the top 10 retrieved results for each query shape.

strating ViewFormer understands multi-view information well by explicitly modeling the correlations for all view pairs in the view set.

3D Shape Retrieval. We visualize the top 10 retrieved shapes for 10 typical queries in Figure 4. The retrieval happens in the ShapeNet Core55 validation set. Each retrieved shape is represented by its random view. We find the top10 results are highly relevant to the query, which means they are in the same category. The 5th shape in the 3rd row maybe confusing, but actually, it is also a cup. Please refer to the supplementary material for more views of this shape.

5. Conclusion

This paper presents ViewFormer, a simple yet effective multi-view 3D shape analysis method. A novel perspective is proposed to organize the multiple views of a 3D shape in a view set, which offers flexibility and avoids assumed relations for views. Based on that, a view set attention

model is devised to learn the pairwise and higher-order correlations of the views in the set adaptively. ViewFormer shows outstanding performances across different datasets and sets new records for recognition and retrieval tasks. But note that the performance gap between point/voxel-based and view-based methods is relatively large. In the future, we plan to explore cross-modal distillation between point/voxel-based and view-based models to narrow the gap.

References

- [1] Umar Asif, Mohammed Bennamoun, and Ferdous A. Sohel. A multi-modal, discriminative and spatially invariant cnn for rgb-d object labeling. *IEEE Transactions on Pattern Analysis and Machine Intelligence*, 40(9):2051–2065, 2018. 5
- [2] Song Bai, Xiang Bai, Zhichao Zhou, Zhaoxiang Zhang, and Longin Jan Latecki. GIFT: A real-time and scalable 3d shape search engine. In *2016 IEEE Conference on Computer Vision and Pattern Recognition, CVPR 2016, Las Vegas, NV, USA, June 27-30, 2016*, pages 5023–5032. IEEE Computer Society, 2016. 6
- [3] Song Bai, Xiang Bai, Zhichao Zhou, Zhaoxiang Zhang, Qi Tian, and Longin Jan Latecki. Gift: Towards scalable 3d shape retrieval. *IEEE Transactions on Multimedia*, PP:1–1, 01 2017. 6
- [4] Andrew Brock, Theodore Lim, J. M. Ritchie, and Nick Weston. Generative and Discriminative Voxel Modeling with Convolutional Neural Networks. *arXiv e-prints*, page arXiv:1608.04236, Aug. 2016. 5
- [5] Angel X. Chang, Thomas A. Funkhouser, Leonidas J. Guibas, Pat Hanrahan, Qi-Xing Huang, Zimo Li, Silvio Savarese, Manolis Savva, Shuran Song, Hao Su, Jianxiang Xiao, Li Yi, and Fisher Yu. Shapenet: An information-rich 3d model repository. *CoRR*, abs/1512.03012, 2015. 6
- [6] Shuo Chen, Tan Yu, and Ping Li. Mvt: Multi-view vision transformer for 3d object recognition. In *British Machine Vision Conference*, 2021. 1, 3, 4, 5, 6, 14
- [7] Songle Chen, Lintao Zheng, Yan Zhang, Zhixin Sun, and Kai Xu. Veram: View-enhanced recurrent attention model for 3d shape classification. *IEEE Transactions on Visualization and Computer Graphics*, 25(12):3244–3257, 2019. 1, 2, 3, 5, 6
- [8] Yanhua Cheng, Rui Cai, Xin Zhao, and Kaiqi Huang. Convolutional fisher kernels for rgb-d object recognition. In *2015 International Conference on 3D Vision*, pages 135–143, 2015. 5
- [9] Junyoung Chung, Caglar Gulcehre, Kyunghyun Cho, and Yoshua Bengio. Empirical evaluation of gated recurrent neural networks on sequence modeling. In *NIPS 2014 Workshop on Deep Learning, December 2014*, 2014. 2
- [10] Alexey Dosovitskiy, Lucas Beyer, Alexander Kolesnikov, Dirk Weissenborn, Xiaohua Zhai, Thomas Unterthiner, Mostafa Dehghani, Matthias Minderer, Georg Heigold, Sylvain Gelly, Jakob Uszkoreit, and Neil Houlsby. An image is worth 16x16 words: Transformers for image recognition at scale. In *International Conference on Learning Representations*, 2021. 3, 6, 7
- [11] Carlos Esteves, Yinshuang Xu, Christine Allen-Blanchette, and Kostas Daniilidis. Equivariant multi-view networks. In *Proceedings of the IEEE/CVF International Conference on Computer Vision (ICCV)*, October 2019. 1, 2, 3, 5
- [12] Yifan Feng, Haoxuan You, Zizhao Zhang, Rongrong Ji, and Yue Gao. Hypergraph neural networks. In *AAAI*, volume 33, pages 3358–3565, 2019. 1, 2, 3, 5, 6
- [13] Yifan Feng, Zizhao Zhang, Xibin Zhao, Rongrong Ji, and Yue Gao. Gvcnn: Group-view convolutional neural networks for 3d shape recognition. In *Proceedings of the IEEE Conference on Computer Vision and Pattern Recognition (CVPR)*, June 2018. 1, 3, 4, 5, 7
- [14] Yue Gao, Yifan Feng, Shuyi Ji, and Rongrong Ji. Hgmn+: General hypergraph neural networks. *IEEE Transactions on Pattern Analysis and Machine Intelligence*, 45(3):3181–3199, 2023. 1, 2, 3, 5, 6
- [15] Abdullah Hamdi, Silvio Giancola, and Bernard Ghanem. Mvtn: Multi-view transformation network for 3d shape recognition. In *Proceedings of the IEEE/CVF International Conference on Computer Vision (ICCV)*, pages 1–11, October 2021. 2, 3, 5
- [16] Zhizhong Han, Honglei Lu, Zhenbao Liu, Chi-Man Vong, Yu-Shen Liu, Matthias Zwicker, Junwei Han, and C. L. Philip Chen. 3d2seqviews: Aggregating sequential views for 3d global feature learning by cnn with hierarchical attention aggregation. *IEEE Transactions on Image Processing*, 28(8):3986–3999, 2019. 1, 2, 3, 5, 6
- [17] Zhizhong Han, Mingyang Shang, Zhenbao Liu, Chi-Man Vong, Yu-Shen Liu, Matthias Zwicker, Junwei Han, and C. L. Philip Chen. Seqviews2seqlabels: Learning 3d global features via aggregating sequential views by rnn with attention. *IEEE Transactions on Image Processing*, 28(2):658–672, 2019. 1, 2, 3, 5, 6
- [18] Kaiming He, Xiangyu Zhang, Shaoqing Ren, and Jian Sun. Deep residual learning for image recognition. In *Proceedings of the IEEE Conference on Computer Vision and Pattern Recognition (CVPR)*, June 2016. 4, 13
- [19] Sepp Hochreiter and Jürgen Schmidhuber. Long Short-Term Memory. *Neural Computation*, 9(8):1735–1780, 11 1997. 2
- [20] Zhengyue Huang, Zhehui Zhao, Hengguang Zhou, Xibin Zhao, and Yue Gao. Deepccfv: Camera constraint-free multi-view convolutional neural network for 3d object retrieval. In *Proceedings of the Thirty-Third AAAI Conference on Artificial Intelligence and Thirty-First Innovative Applications of Artificial Intelligence Conference and Ninth AAAI Symposium on Educational Advances in Artificial Intelligence*, AAAI’19/IAAI’19/EAAI’19. AAAI Press, 2019. 5
- [21] Edward Johns, Stefan Leutenegger, and J. Davison Andrew. Pairwise decomposition of image sequences for active multi-view recognition. In *2016 IEEE Conference on Computer Vision and Pattern Recognition (CVPR)*, 2016. 3
- [22] Asako Kanezaki, Yasuyuki Matsushita, and Yoshifumi Nishida. Rotationnet: Joint object categorization and pose estimation using multiviews from unsupervised viewpoints. In *Proceedings of the IEEE Conference on Computer Vision and Pattern Recognition (CVPR)*, June 2018. 2, 3, 5, 6, 13

- [23] Naoki Katsura. Pytorch cosineannealing with warmup restarts. <https://github.com/katsura-jp/pytorch-cosine-annealing-with-warmup>, 2021. 12
- [24] Alex Krizhevsky, Ilya Sutskever, and Geoffrey E Hinton. Imagenet classification with deep convolutional neural networks. In F. Pereira, C.J. Burges, L. Bottou, and K.Q. Weinberger, editors, *Advances in Neural Information Processing Systems*, volume 25. Curran Associates, Inc., 2012. 4, 13, 14
- [25] Kevin Lai, Liefeng Bo, Xiaofeng Ren, and Dieter Fox. A large-scale hierarchical multi-view rgb-d object dataset. In *2011 IEEE International Conference on Robotics and Automation*, pages 1817–1824, 2011. 5, 6
- [26] Yongcheng Liu, Bin Fan, Shiming Xiang, and Chunhong Pan. Relation-shape convolutional neural network for point cloud analysis. In *IEEE Conference on Computer Vision and Pattern Recognition (CVPR)*, pages 8895–8904, 2019. 1, 5
- [27] Ilya Loshchilov and Frank Hutter. Decoupled weight decay regularization. In *International Conference on Learning Representations*, 2019. 12
- [28] Chao Ma, Yulan Guo, Jungang Yang, and Wei An. Learning multi-view representation with lstm for 3-d shape recognition and retrieval. *IEEE Transactions on Multimedia*, 21(5):1169–1182, 2019. 1, 2, 3
- [29] Chao Ma, Yulan Guo, Jungang Yang, and Wei An. Learning multi-view representation with lstm for 3-d shape recognition and retrieval. *IEEE Transactions on Multimedia*, 21(5):1169–1182, 2019. 5
- [30] Xu Ma, Can Qin, Haoxuan You, Haoxi Ran, and Yun Fu. Rethinking network design and local geometry in point cloud: A simple residual MLP framework. In *International Conference on Learning Representations*, 2022. 1, 5
- [31] Daniel Maturana and Sebastian Scherer. Voxnet: A 3d convolutional neural network for real-time object recognition. In *2015 IEEE/RSJ International Conference on Intelligent Robots and Systems (IROS)*, pages 922–928, 2015. 1, 5
- [32] Charles R. Qi, Hao Su, Kaichun Mo, and Leonidas J. Guibas. Pointnet: Deep learning on point sets for 3d classification and segmentation. In *Proceedings of the IEEE Conference on Computer Vision and Pattern Recognition (CVPR)*, July 2017. 1
- [33] Charles R. Qi, Hao Su, Matthias Nießner, Angela Dai, Mengyuan Yan, and Leonidas J. Guibas. Volumetric and multi-view cnns for object classification on 3d data. In *2016 IEEE Conference on Computer Vision and Pattern Recognition (CVPR)*, pages 5648–5656, 2016. 1, 5
- [34] Charles Ruizhongtai Qi, Li Yi, Hao Su, and Leonidas J Guibas. Pointnet++: Deep hierarchical feature learning on point sets in a metric space. In I. Guyon, U. Von Luxburg, S. Bengio, H. Wallach, R. Fergus, S. Vishwanathan, and R. Garnett, editors, *Advances in Neural Information Processing Systems*, volume 30. Curran Associates, Inc., 2017. 1, 5
- [35] Mohammad Muntasir Rahman, Yanhao Tan, Jian Xue, and Ke Lu. Rgb-d object recognition with multimodal deep convolutional neural networks. In *2017 IEEE International Conference on Multimedia and Expo (ICME)*, pages 991–996, 2017. 5
- [36] Sebastian Ruder. An overview of gradient descent optimization algorithms., 2016. cite arxiv:1609.04747Comment: Added derivations of AdaMax and Nadam. 12
- [37] Kripasindhu Sarkar, Basavaraj Hampiholi, Kiran Varanasi, and Didier Stricker. Learning 3d shapes as multi-layered height-maps using 2d convolutional networks. *ArXiv*, abs/1807.08485, 2018. 2, 3
- [38] Manolis Savva, Fisher Yu, Hao Su, Asako Kanezaki, Takahiko Furuya, Ryutarou Ohbuchi, Zhichao Zhou, Rui Yu, Song Bai, Xiang Bai, Masaki Aono, Atsushi Tatsuma, S. Theros, A. Axenopoulos, G. Th. Papadopoulos, P. Daras, Xiao Deng, Zhouhui Lian, Bo Li, Henry Johan, Yijuan Lu, and Sanjeev Mk. Large-Scale 3D Shape Retrieval from ShapeNet Core55. In Ioannis Pratikakis, Florent Dupont, and Maks Ovsjanikov, editors, *Eurographics Workshop on 3D Object Retrieval*. The Eurographics Association, 2017. 3, 6
- [39] Hang Su, Subhransu Maji, Evangelos Kalogerakis, and Erik Learned-Miller. Multi-view convolutional neural networks for 3d shape recognition. In *2015 IEEE International Conference on Computer Vision (ICCV)*, pages 945–953, 2015. 1, 3, 4, 5, 6, 7
- [40] Jong-Chyi Su, Matheus Gadelha, Rui Wang, and Subhransu Maji. A deeper look at 3d shape classifiers. In Laura Leal-Taixé and Stefan Roth, editors, *Computer Vision – ECCV 2018 Workshops*, pages 645–661, Cham, 2018. Springer International Publishing. 1, 3, 5, 7
- [41] Hugues Thomas, Charles R. Qi, Jean-Emmanuel Deschaud, Beatriz Marcotegui, Francois Goulette, and Leonidas J. Guibas. Kpconv: Flexible and deformable convolution for point clouds. In *Proceedings of the IEEE/CVF International Conference on Computer Vision (ICCV)*, October 2019. 1, 5
- [42] Laurens van der Maaten and Geoffrey Hinton. Visualizing data using t-sne. *Journal of Machine Learning Research*, 9(86):2579–2605, 2008. 8
- [43] Ashish Vaswani, Noam Shazeer, Niki Parmar, Jakob Uszkoreit, Llion Jones, Aidan N Gomez, Łukasz Kaiser, and Illia Polosukhin. Attention is all you need. In I. Guyon, U. Von Luxburg, S. Bengio, H. Wallach, R. Fergus, S. Vishwanathan, and R. Garnett, editors, *Advances in Neural Information Processing Systems*, volume 30. Curran Associates, Inc., 2017. 2, 3, 4, 7
- [44] Chu Wang, Marcello Pelillo, and Kaleem Siddiqi. Dominant set clustering and pooling for multi-view 3d object recognition. In *British Machine Vision Conference*, 06 2019. 1, 3, 4, 5, 7
- [45] Yue Wang, Yongbin Sun, Ziwei Liu, Sanjay E. Sarma, Michael M. Bronstein, and Justin M. Solomon. Dynamic graph cnn for learning on point clouds. *ACM Transactions on Graphics (TOG)*, 2019. 1, 5
- [46] Xin Wei, Ruixuan Yu, and Jian Sun. View-gcn: View-based graph convolutional network for 3d shape analysis. In *Proceedings of the IEEE/CVF Conference on Computer Vision and Pattern Recognition (CVPR)*, June 2020. 1, 2, 3, 5, 6, 13
- [47] Xin Wei, Ruixuan Yu, and Jian Sun. Learning view-based graph convolutional network for multi-view 3d shape analysis. *IEEE Transactions on Pattern Analysis and Machine Intelligence*, pages 1–17, 2022. 1, 2, 3, 5, 6

- [48] Wenxuan Wu, Zhongang Qi, and Li Fuxin. Pointconv: Deep convolutional networks on 3d point clouds. In *Proceedings of the IEEE/CVF Conference on Computer Vision and Pattern Recognition (CVPR)*, June 2019. [1](#)
- [49] Zhirong Wu, Shuran Song, Aditya Khosla, Fisher Yu, Linguang Zhang, Xiaoou Tang, and Jianxiong Xiao. 3d shapenets: A deep representation for volumetric shapes. In *Proceedings of the IEEE Conference on Computer Vision and Pattern Recognition (CVPR)*, June 2015. [1](#), [5](#)
- [50] Tiange Xiang, Chaoyi Zhang, Yang Song, Jianhui Yu, and Weidong Cai. Walk in the cloud: Learning curves for point clouds shape analysis. In *Proceedings of the IEEE/CVF International Conference on Computer Vision (ICCV)*, pages 915–924, October 2021. [1](#), [5](#)
- [51] Yong Xu, Chaoda Zheng, Ruotao Xu, Yuhui Quan, and Haibin Ling. Multi-view 3d shape recognition via correspondence-aware deep learning. *IEEE Transactions on Image Processing*, 30:5299–5312, 2021. [1](#), [2](#), [3](#), [5](#), [14](#)
- [52] Xu Yan, Chaoda Zheng, Zhen Li, Sheng Wang, and Shuguang Cui. Pointasnl: Robust point clouds processing using nonlocal neural networks with adaptive sampling. In *Proceedings of the IEEE/CVF Conference on Computer Vision and Pattern Recognition (CVPR)*, June 2020. [1](#)
- [53] Ze Yang and Liwei Wang. Learning relationships for multi-view 3d object recognition. In *Proceedings of the IEEE/CVF International Conference on Computer Vision (ICCV)*, October 2019. [2](#), [3](#), [5](#), [6](#)
- [54] Tan Yu, Jingjing Meng, Ming Yang, and Junsong Yuan. 3d object representation learning: A set-to-set matching perspective. *IEEE Transactions on Image Processing*, 30:2168–2179, 2021. [1](#), [3](#), [4](#), [7](#), [14](#)
- [55] Tan Yu, Jingjing Meng, and Junsong Yuan. Multi-view harmonized bilinear network for 3d object recognition. In *Proceedings of the IEEE Conference on Computer Vision and Pattern Recognition (CVPR)*, June 2018. [1](#), [3](#), [4](#), [5](#), [7](#), [14](#)
- [56] Zizhao Zhang, Haojie Lin, Xibin Zhao, Rongrong Ji, and Yue Gao. Inductive multi-hypergraph learning and its application on view-based 3d object classification. *IEEE Transactions on Image Processing*, 27(12):5957–5968, 2018. [1](#), [2](#), [3](#), [5](#), [6](#)
- [57] Hengshuang Zhao, Li Jiang, Chi-Wing Fu, and Jiaya Jia. Pointweb: Enhancing local neighborhood features for point cloud processing. In *Proceedings of the IEEE/CVF Conference on Computer Vision and Pattern Recognition (CVPR)*, June 2019. [1](#)
- [58] Hengshuang Zhao, Li Jiang, Jiaya Jia, Philip H.S. Torr, and Vladlen Koltun. Point transformer. In *Proceedings of the IEEE/CVF International Conference on Computer Vision (ICCV)*, pages 16259–16268, October 2021. [1](#)
- [59] Yin Zhou and Oncel Tuzel. Voxelnet: End-to-end learning for point cloud based 3d object detection. In *Proceedings of the IEEE Conference on Computer Vision and Pattern Recognition (CVPR)*, June 2018. [1](#)

A. Additional Analysis

We provide additional analysis to the proposed approach, including network optimization, shallow convolution operations in Initializer, the number of views, learning efficiency, the architecture of the view set encoder, the performances gains delivered by the devised encoder, and the effect of patch-level feature interactions.

A.1. Network Optimization

We adopt a 2-stage training strategy to optimize the proposed model and verify its effectiveness through the following experiments.

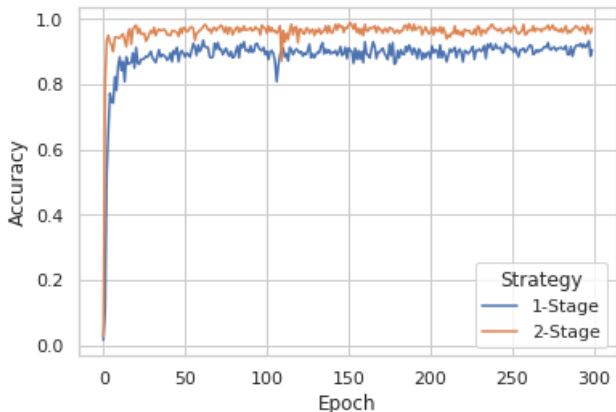


Figure 5: Comparison of instance accuracy on ModelNet40 when using 1-stage and 2-stage optimization.

1-Stage vs. 2-Stage. We compare the effectiveness of 1-stage and 2-stage optimization on ModelNet40. For 2-stage optimization, Initializer is trained individually on the dataset, then the pre-trained weights of Initializer are loaded into ViewFormer to be optimized with other modules jointly. The 1-stage optimization means ViewFormer learns in an end-to-end way and all parameters are randomly initialized. Figure 5 shows the recognition accuracy achieved by 2-stage optimization is significantly better than that of 1-stage training. The results demonstrate ViewFormer receives gains from the well-initialized view representations provided by the first stage of learning.

Training Details. For Initializer, we train it 30 epochs on the target dataset using SGD [36], with an initial learning rate 0.01 and CosineAnnealingLR scheduler. After that, the pre-trained weights of Initializer are loaded into ViewFormer to be optimized with other modules jointly. Specifically, ViewFormer is trained 300 epochs on the target dataset using AdamW [27], with an initial peak learning rate 0.001 and CosAnnealingWarmupRestartsLR scheduler [23]. The restart interval is 100 epochs and the warmup happens in the first 5 epochs of each interval. The learning

rate increases to the peak linearly during warmup and the peak decays by 40% after each interval. The learning rate curve is visualized in Figure 6.

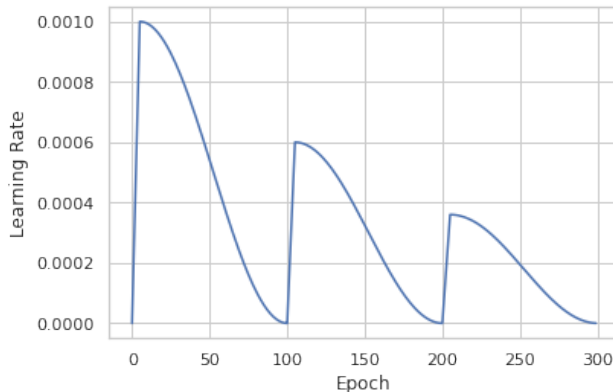


Figure 6: The learning rate curve for optimizing ViewFormer.

A.2. Shallow Convolution Operations in Initializer

We investigate the performances of ViewFormer when deploying shallow convolution operations as Initializer, e.g., 1- and 2-layer convolution. Table 10 and 11 explains their specific configurations. Due to the increased number of strides, 2-layer convolution has much lower parameters than 1-layer operation. However, ViewFormer with shallow convolution initializations does not lead to decent 3D shape recognition. The best instance accuracy is 93.7%, much lower than 98.8% given by ViewFormer with lightweight CNN (AlexNet) Initializer, suggesting lightweight CNNs are reasonable choices for the Init module.

View Size	$224 \times 224 \times 3$
1st Conv	Conv2d(in=3,out=64,k=7,s=2,p=3) BatchNorm2d(num=64) ReLU(inplace=True) MaxPool2d(k=3, s=2, p=1)
Total #Params	102.8 M
Class Acc.	90.1%
Inst. Acc.	92.5%

Table 10: Configuration of the 1-layer convolution in Initializer.

A.3. Ablation Studies

We conduct additional ablations to ViewFormer on ModelNet40, including the number of views used, the difference

View Size	$224 \times 224 \times 3$
1st Conv	Conv2d(in=3, out=64, k=7, s=2, p=3)
	BatchNorm2d(num=64)
	ReLU(inplace=True)
	MaxPool2d(k=3, s=2, p=1)
2nd Conv	Conv2d(in=64, out=32, k=3, s=2, p=1)
	BatchNorm2d(num=32)
	ReLU(inplace=True)
Total #Params	12.9 M
Class Acc.	88.9%
Inst. Acc.	93.7%

Table 11: Configuration of the 2-layer convolution in Initializer.

between various models using the same initializer module, the effect of pre-trained initializer and the performance gain brought by the encoder. We hope the studies can provide more insights on the design choices.

Effect of the Number of Views. We investigate the effect of the number of views on the recognition performance, shown in Table 12. There are up to 20 views for each 3D shape and we randomly select M views for each shape for training and evaluation, where $M \in \{1, 4, 8, 12, 16, 20\}$. When $M = 1$, the problem is equivalent to single-view object recognition, so there is no interaction among views. In this case, a lightweight ResNet18 [18] is trained for recognition and it achieves 89.0% mean class accuracy and 91.8% instance accuracy. When increasing the number of views, the performances are quickly improved. For instance, after aggregating the correlations from 4 views, ViewFormer lifts 8.4% and 5.3% absolute points in class and instance accuracy, respectively. But exploiting more views does not necessarily result in better accuracy. The 8-view ViewFormer reaches 98.0% class accuracy and 98.8% overall accuracy, outperforming 12- and 16-view versions. The performance is optimal when exploiting all 20 views and we choose this version to compare with other view-based methods.

#views	Class Acc. (%)	Inst. Acc. (%)
1	89.0	91.8
4	97.4	97.1
8	98.0	98.8
12	97.5	97.6
16	97.7	98.3
20	98.9	98.8

Table 12: Ablation study: the number of views.

Different Methods Using Same Initializer. To be fair, we use same Initializer for different methods to inspect their recognition accuracies on ModelNet40. The chosen methods are representative baselines, RotationNet [22] and View-GCN [46]. The results in Table 13 show ViewFormer can achieve higher-level performance no matter the view representations are initialized by AlexNet [24] or ResNet50 [18], exceeding View-GCN(AlexNet) and View-GCN(ResNet) by 1.6% and 1.5%, respectively. The results also indicate the proposed approach is better at grasping multi-view information for recognition since the initialized view features are identical.

Method	Initializer	Inst. Acc. (%)
RotationNet		96.4
View-GCN	AlexNet	97.2
ViewFormer		98.8
RotationNet		96.9
View-GCN	ResNet50	97.3
ViewFormer		98.8

Table 13: Ablation study: different methods using a same Initializer.

Learning Efficiency. We explore the learning efficiency of ViewFormer by freezing the weights of the pre-trained Initializer. Figure 7 displays the recognition accuracy curves of ViewFormer variants with different initializers on ModelNet40 during training. Regardless of Initializer used, all variants’ performances soared after a short training and approached the highest. For instance, ViewFormer with ResNet34 Initializer reaches 97.6% instance accuracy after only 2-epoch learning, while View-GCN [46] achieves the same performance with 7.5x longer optimization. The results reflect the proposed method has higher learning efficiency than the previous state of the art.

The Architecture of Encoder. We provide ablations to justify the design choices of Encoder. The controlled variables of Encoder are the number of attention blocks (#Blocks), the number of attention heads in MSA (#Heads), the widening ratio of MLP hidden layer ($Ratio_{mlp}$) and the dimension of the view representations (Dim_{view}). The mean class accuracy and instance accuracy of ViewFormer with different encoder structures are compared in Table 14. All design variants show high-level performances and surpass the existing state of the art. Surprisingly, the encoder consisting of only 2 attention blocks can facilitate ViewFormer to achieve 99.0% overall accuracy. The results are in line with expectations as the size of a view set is relatively small thus, it is unnecessary to design a very complex encoder. At the same time, it is inspiring that pairwise and higher-order correlations of elements in the view set can be enriched and well

#Blocks	2	2	2	2	4	4	4	4	6	6	6	6
#Heads	6	8	6	8	6	8	6	8	6	8	6	8
Ratio _{mlp}	2	2	4	4	2	2	4	4	2	2	4	4
Dim _{view}	384	512	384	512	384	512	384	512	384	512	384	512
#Params (M)	2.7	4.8	3.9	6.9	5.0	9.0	7.4	13.2	7.4	13.2	11.0	19.5
ModelNet40												
Class Acc. (%)	98.8	98.7	98.4	97.2	97.4	98.9	99.1	98.2	98.7	98.2	98.4	98.1
Inst. Acc. (%)	99.0	98.8	98.5	98.1	97.6	98.8	98.5	98.5	98.3	98.3	98.1	98.3

Table 14: Ablation Study: the architecture of Encoder.

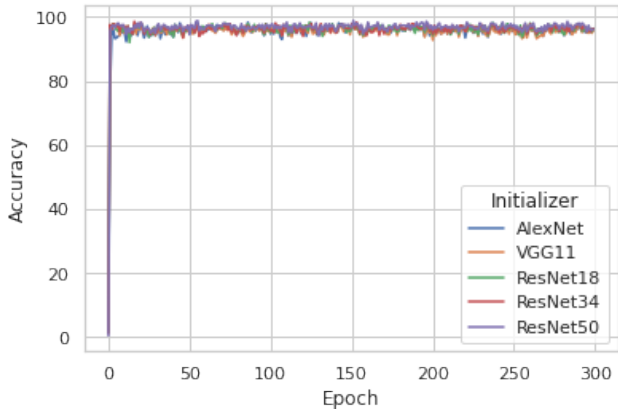


Figure 7: Learning efficiency of ViewFormer.

grasped by a shallow encoder. Finally, we select the design that takes *the second place* in both mean class and instance accuracy, namely #Blocks = 4, #Heads = 8, Ratio_{mlp} = 2 and Dim_{view} = 512.

Performance Gains Delivered by Our Encoder. We investigate the performance gains delivered by the devised view set encoder. First, the initializer is individually trained to recognize 3D shapes in ModelNet40. Second, the devised encoder is appended upon the pre-trained initializer to further capture the feature interactions among views. The chosen architecture for encoder is #Blocks = 2, #Heads = 6, Ratio_{mlp} = 2, Dim_{view} = 384, seen in Table 14. Table 15 compares the number of parameters and performances of different configurations described above. Notable performance gains are obtained by the proposed view set encoder over different initializers. For example, by appending 2 attention blocks on the AlexNet initializer, our model achieves 18.2% and 14.9% absolute improvements for mean class accuracy and instance accuracy. In contrast, the introduced 2.7M parameters only account for 6.4% of that in AlexNet [24].

Effect of Patch-level Feature Correlations. Some other methods also consider fine-grained patch-level interactions [55, 54, 6, 51]. They believe multi-view information flow can be enhanced by integrating patch-level features. In

Module	#Params (M)	Class Acc. (%)	Inst. Acc. (%)
AlexNet	42.3	80.6	85.1
+ 2 Attn. Blocks	2.7	98.8	99.0
ResNet18	11.2	88.7	91.8
+ 2 Attn. Blocks	2.7	98.1	97.8

Table 15: Ablation study: the performance gains brought by the devised encoder over Initializer.

Variants	Class Acc. (%)	Inst. Acc. (%)
w/ patch	98.1	98.1
w/o patch	98.9	98.8

Table 16: Ablation study: effect of the patch-level correlations.

this work, we examine the effect of patch-level feature correlations by injecting them into each attention block of the encoder. The results in Table 16 show injecting patch-level features is redundant and unnecessary, disturbs the multi-view information understanding and decreases the performance slightly. But whether the patch-level correlations are integrated or not, ViewFormer maintains high-level performances (98.0+% accuracies) and surpasses all existing models.

B. Visualizations

Multi-view Attention in Colored Lines. We randomly select a 3D shape that is a nightstand, then visualize the multi-view correlations of eight views of this shape, referring to Figure 8. The correlations are represented by the attention scores emitted by the last attention block of ViewFormer. The scores are normalized to map to the color bar on the far right of the figure. Our model distributes more weights to 2nd, 3rd, 6th views from the 5th one. The results seem reasonable since these views are more discriminative according to visual appearances.

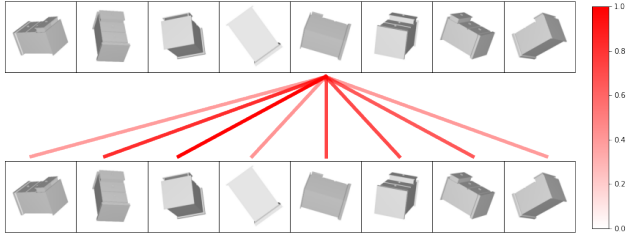


Figure 8: Visualization of multi-view attention of 8 views of a nightstand in colored lines.

Another 3D shape is randomly selected to demonstrate multi-view attention. The selected shape is a range hood. In Figure 9, we visualize the interactions of all view pairs for the shape. The purpose is to let readers feel the flexibility of organizing multiple views of a 3D shape into a set and the powerful capability of view set attention in modeling the correlations among elements in a set.

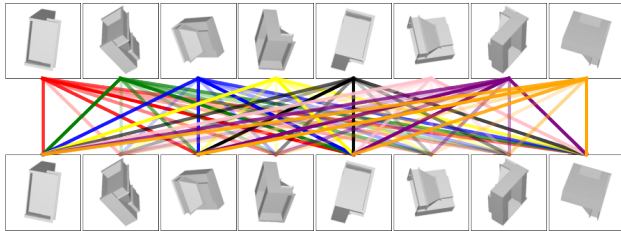


Figure 9: Visualization of multi-view attention for all view pairs of a range hood in colorful lines.

Multiple Views of a Retrieved Shape. In Figure 4 of the main paper, the retrieved shape in the 5th column of the 3rd row may be confusing since one may not be able to determine whether it belongs to the same class as the query. To this end, we pinpoint the shape in the dataset and find more views of it, shown in Figure 10. After observing these views, we can infer this shape is a cup, so it is of the same class as the query. The example also demonstrates a central problem of multi-view 3D shape analysis, how to integrate multi-view information effectively.

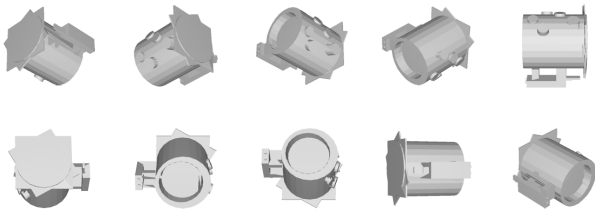


Figure 10: Multiple views of a retrieved shape.